

Electronic Supplementary Information

Full and gradient structural colouration by lattice amplified gallium nitride Mie-resonators

Jaehyuck Jang^{†,‡}, Trevon Badloe^{‡,‡,‡}, Young Chul Sim^{§,‡}, Younghwan Yang[‡], Jungho Mun[†],
Taejun Lee[‡], Yong-Hoon Cho^{§,*}, and Junsuk Rho^{†,‡,‡,‡,‡,‡,‡}

[†]Department of Chemical Engineering, Pohang University of Science and Technology
(POSTECH), Pohang 37673, Republic of Korea

[‡]Department of Mechanical Engineering, Pohang University of Science and Technology
(POSTECH), Pohang 37673, Republic of Korea

[§]Department of Physics and KI for the NanoCentury, Korea Advanced Institute of Science
and Technology (KAIST), Daejeon 34141, Republic of Korea

[‡]National Institute of Nanomaterials Technology (NINT), Pohang 37673, Republic of Korea

[‡]These authors contributed equally to this work

*Corresponding author. E-mail: jsrho@postech.ac.kr & yhc@kaist.ac.kr

Supplementary Note 1 – Measured refractive index of GaN and a-Si:H

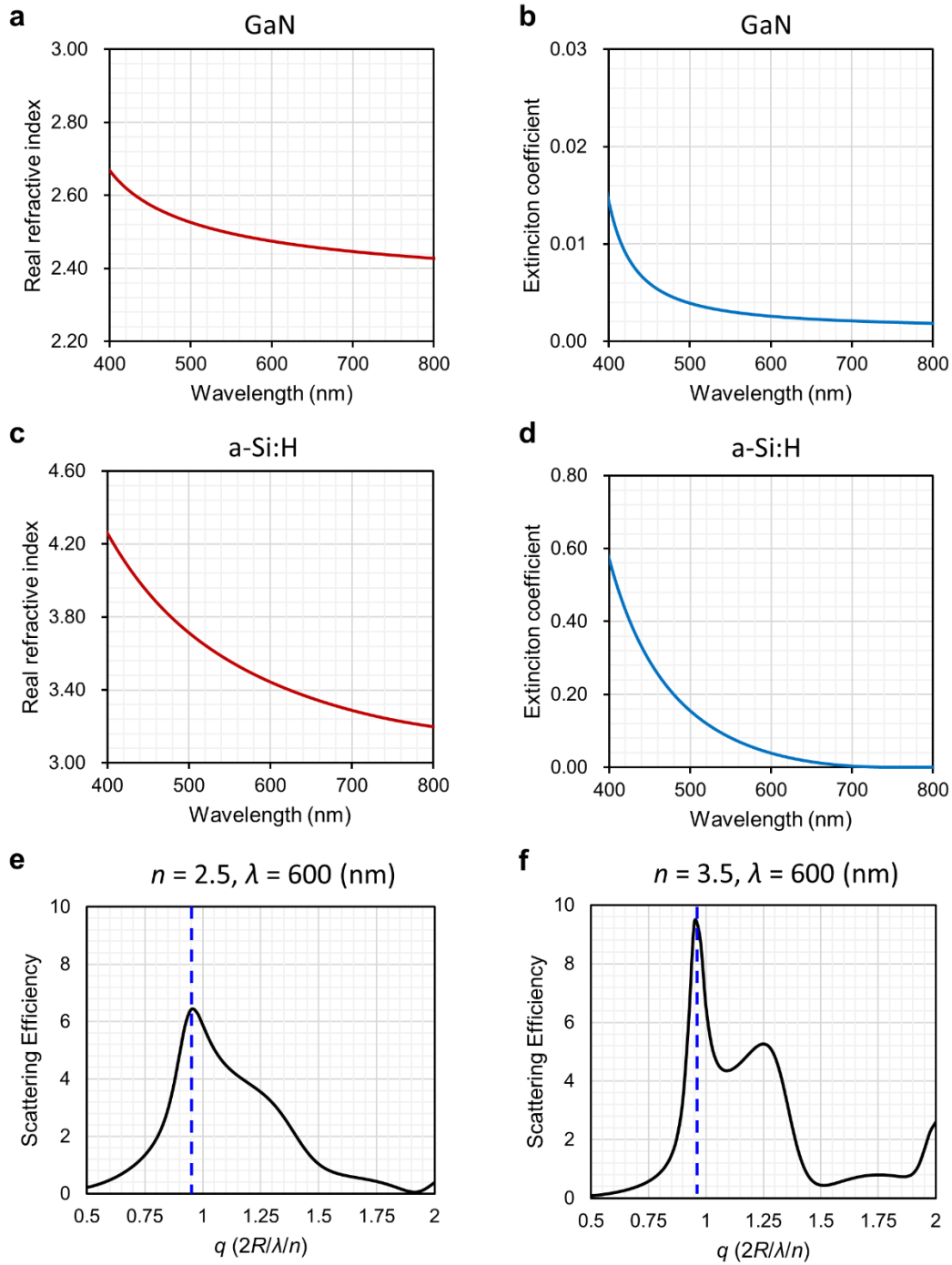


Figure S1. Measured refractive index of gallium nitride (GaN) and hydrogenated amorphous silicon (a-Si:H). (a) Real and (b) imaginary part of the refractive index of GaN. (c) Real and (d) imaginary part of the refractive index of a-Si:H. Scattering efficiency of a dielectric sphere with refractive index (e) $n = 2.5$ and (f) $n = 3.5$ under $\lambda = 600$ nm wavelength illumination. Blue-dashed line: MD. Higher refractive index supports stronger scattering efficiency.

Supplementary Note 2 – Substrate effect

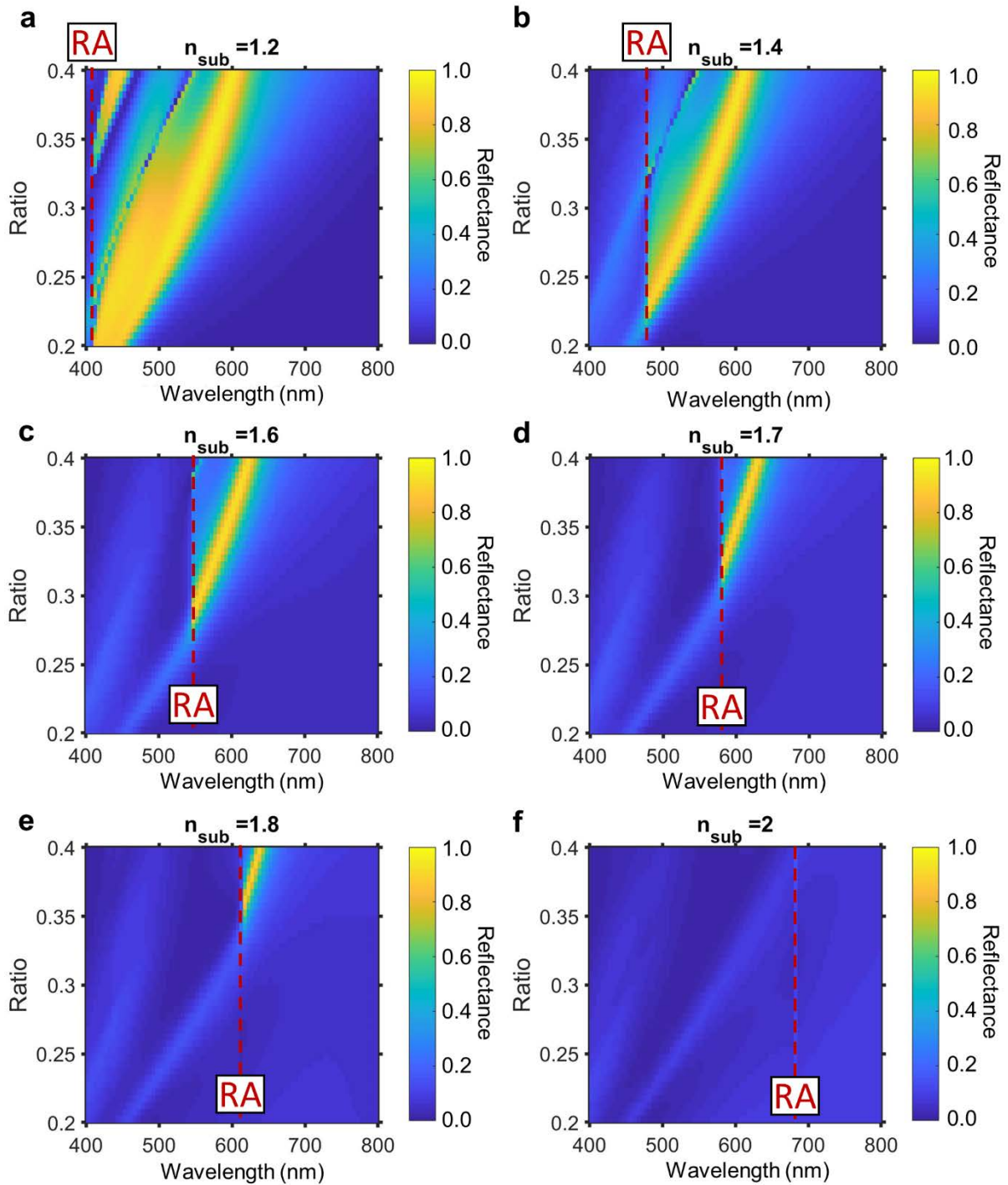


Figure S2. GMR condition bounded by substrate index. Reflection spectra of the proposed GaN metasurfaces at the different refractive index of the substrates n_{sub} set to be (a) 1.2, (b) 1.4, (c) 1.6, (d) 1.7, (e) 1.8, and (f) 2. Red-dashed line: Rayleigh anomaly (RA).

Supplementary Note 3. Minimum refractive index of Mie-scatterers for structural colour

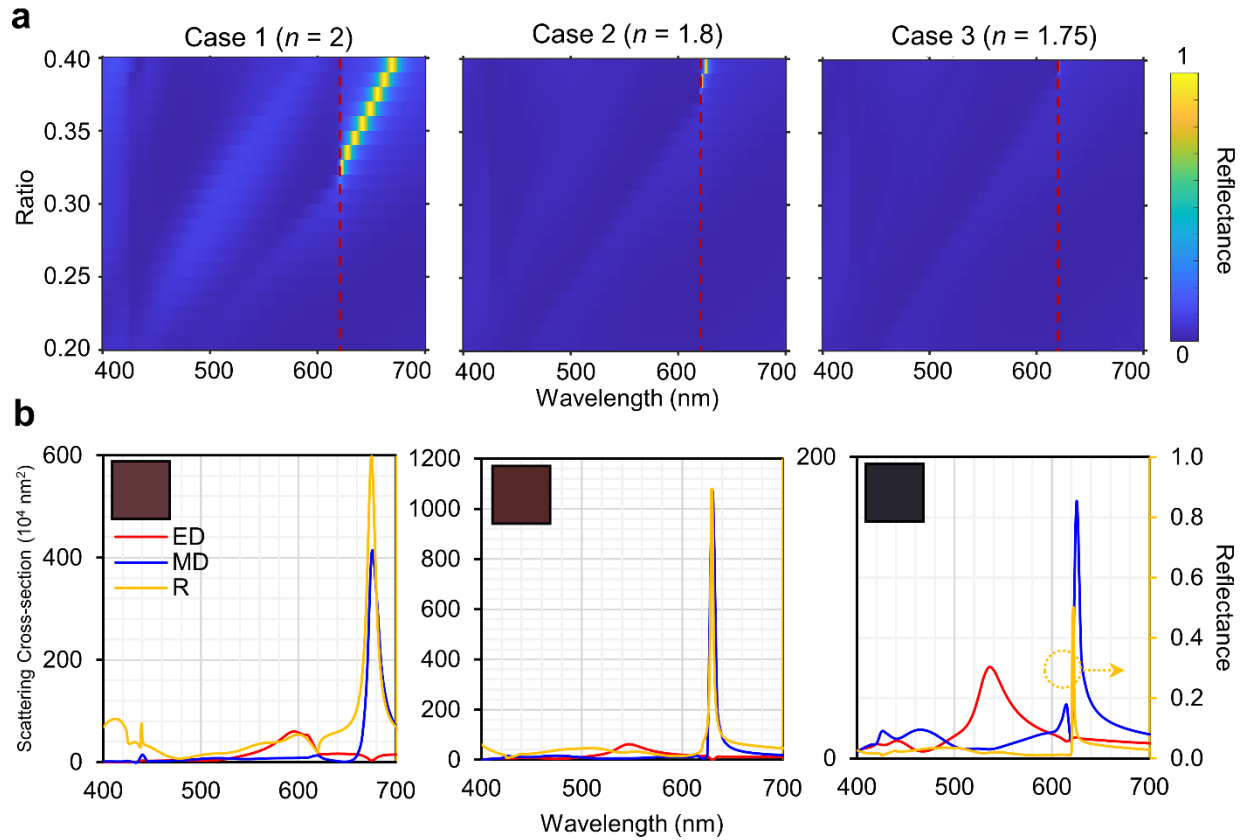


Figure S3. Optical responses for arrays of Mie-scatterers with different refractive index. (a) Simulated reflection spectra for a nanorod array on a silica substrate with P (period) = 425 nm, f (ratio) = 0.2 ~ 0.4, and h (height) = 400nm with n (refractive index) = 2 (Case 1), $n = 1.8$ (Case 2), and $n = 1.75$ (Case 3). Dashed line: RA. (b) Scattering cross section and reflection spectrum of Cases 1, 2, and 3 when $f = 0.4$. Red: ED; Blue: MD; Yellow: Reflection; Insets: colour swatches corresponding to each reflection spectrum.

Three cases of cylindrical nanorods array on a silica substrate ($n = 1.46$) with P (period) = 425 nm, f (ratio) = 0.2 ~ 0.4, and h (height) = 400nm with n (refractive index) = 2 (Case 1), $n = 1.8$ (Case 2), and $n = 1.75$ (Case 3) are investigated. From the multipole expansions with $f = 0.4$, the dominant MD peak is at $\lambda = 670$ nm, 630 nm, and 625 nm, for case 1, 2, and 3, respectively. The MD peak is blue-shifted as the refractive index of the constituent material decreases. Since the resonance can be excited within the required regime governed by Equation 3 ($\lambda_{RA} = 620.5$ nm; dashed line in Fig. S3a), all three cases are candidates to satisfy the conditions for lattice-enhanced structural coloration.

However, the minimum index to produce structure colour should take more factors into account. First, the reflection spectrum must be high and broad enough to render the desired colours, regardless of if the designed scatterers are enhanced by the lattice resonance. In Case 3, the MD is amplified through the lattice resonance, yet produces dull and muddy colours because the resonance peak is too sharp, so is outweighed by the background response (right side of Fig. S3b). For efficient and vivid colouration, the full width at half maximum (FWHM) should be further considered with regards to the reflection at off resonant wavelengths. Secondly, the excitation wavelength of the multipolar modes of a Mie-scatter differs greatly by the geometry of the scatterer, so the feasibility of a certain material is uncertain until all physically possible geometries of scatterer with that material are fully explored. Moreover, the substrate and background medium of the scatterers affect the radiation modes as well as the location of the RA. Lastly, the dispersion of the refractive index was not considered since most dielectric materials have a standard dispersion in the visible regime. If the material has anomalous dispersion, the resonance peak would not follow the trend as seen in Cases 1 to 3.

Therefore, in this case, i.e. an i) infinite array of ii) cylindrical nanorods, on iii) a silica substrate (chosen as it is the most commonly used), iv) with a background medium of air, and v) a normal dispersion in the visible regime, the minimum refractive index of the Mie-scatterers to produce structural coloration through lattice-enhanced reflection is around 1.8.

Supplementary Note 4 – Fabrication process of the GaN metasurfaces

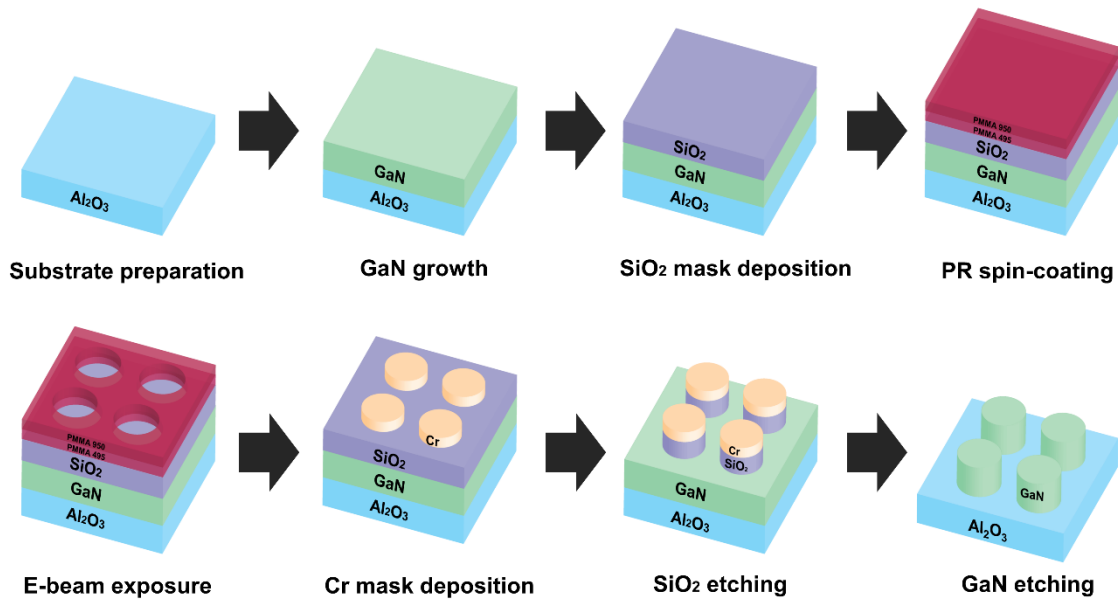


Figure S4. Fabrication process of the GaN metasurfaces. A two-step etching processes is required to produce the designed GaN nanorods.

The fabrication process of the GaN metasurfaces begins with the preparation of a polished sapphire substrate. A 250 nm-thick GaN layer is then grown using metal-organic chemical vapor deposition (MOCVD) in a closed-coupled-showerhead reactor (Thomas Swan, 3X2"). During the deposition process, H_2 precursors are used to transport trimethylgallium (TMGa). After the MOCVD process, a 100 nm-thick layer of silicon oxide (SiO_2) is sequentially deposited on the GaN film using an electron beam evaporator (KVT, KVE-ENS4004). A double-layer photoresist is spin-coated on the film, first a layer of 495-polymethylmethacrylate (PMMA) and then a layer of 950-PMMA. An E-spacer is coated on the baked resist for 30 seconds at 3000 rpm to reduce the error induced by electron charging. This E-spacer layer is not illustrated in the figure for clarity. The coated resist is exposed using electron beam lithography (ELIONIX, ELS-7800, 80kV, 50kV) at an 80 kV acceleration voltage with a beam current of 100 pA. The different molecular weights of 495-PMMA and 950-PMMA occur undercut when they are developed with a solution (4-Methylpentan-2one:2-propanol = 1:3, Micro Chem). A 15 nm-thick chrome mask is deposited with an electron-beam evaporator with the vacuum condition kept at 10^{-7} Torr to reduce side wall deposition. The lift-off process is conducted with hot acetone (60 °C) for 6 hours,

revealing a 15 nm-thick Cr mask. The pattern is transferred to the hard SiO₂ mask and GaN nanorod using an inductively coupled-plasma reactive ion etching (ICP-RIE) system. Finally, the designed GaN metasurfaces are formed by removing the SiO₂ using buffered oxide etchant (BOE).

Supplementary Note 5 – Colour palettes of the GaN metasurfaces

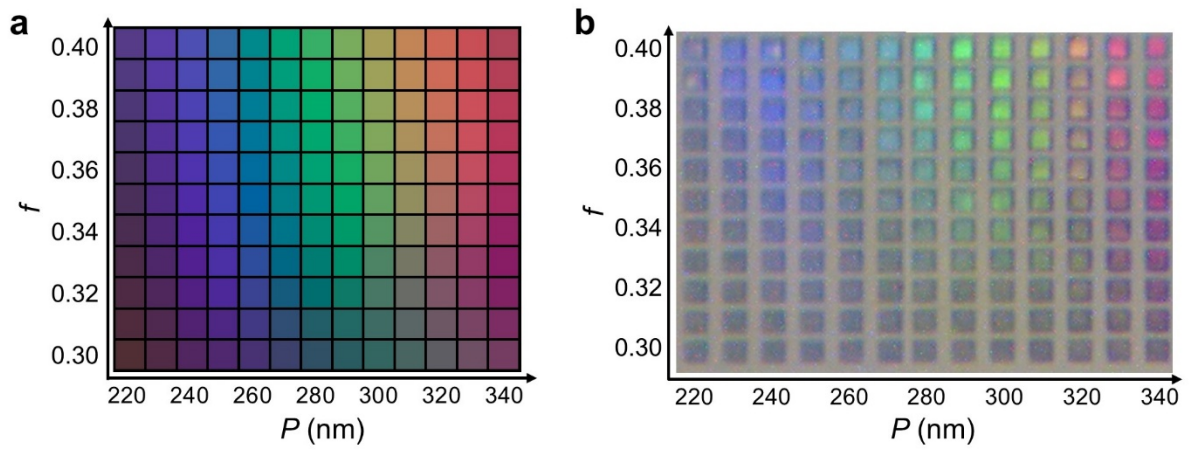


Figure S5. Colour palettes. (a) Simulated and (b) fabricated colour palette of the GaN metasurfaces with $P = 220 - 340$ nm and $f = 0.30 - 0.40$.

Supplementary Note 6 – Visualisation of the HSV colour space

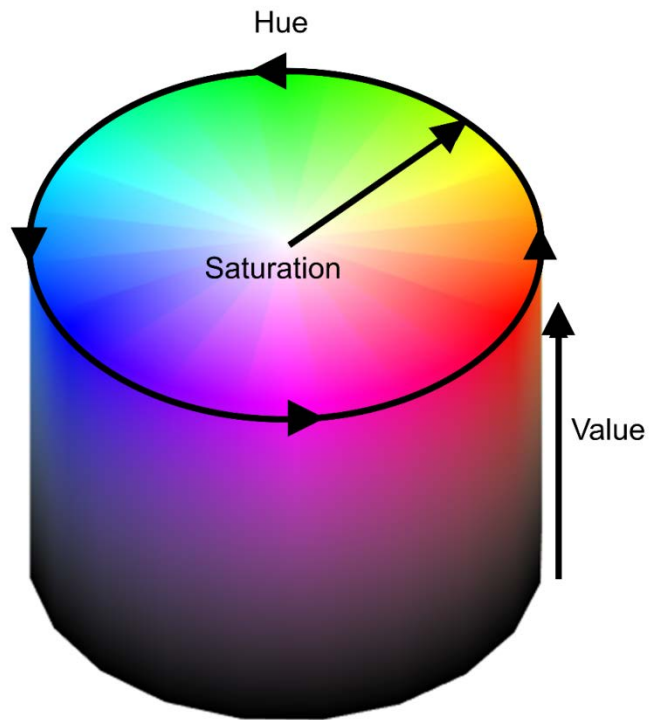


Figure S6. Visualisation of the HSV colour space. Hue rotates through spectral colours from red at 0, through orange, yellow, green, and to blue, continuing through extra spectral colours such as magenta and pink and back to red at 1. Saturation denotes the amount of hue, from 0 at the centre (corresponding to a shade of grey), to 1 at the edge of the cylinder. Value represents the brightness or intensity of the colour from 0 (black) to 1 (fully bright colour).

Supplementary Note 7 – Effective number of structures in arrays

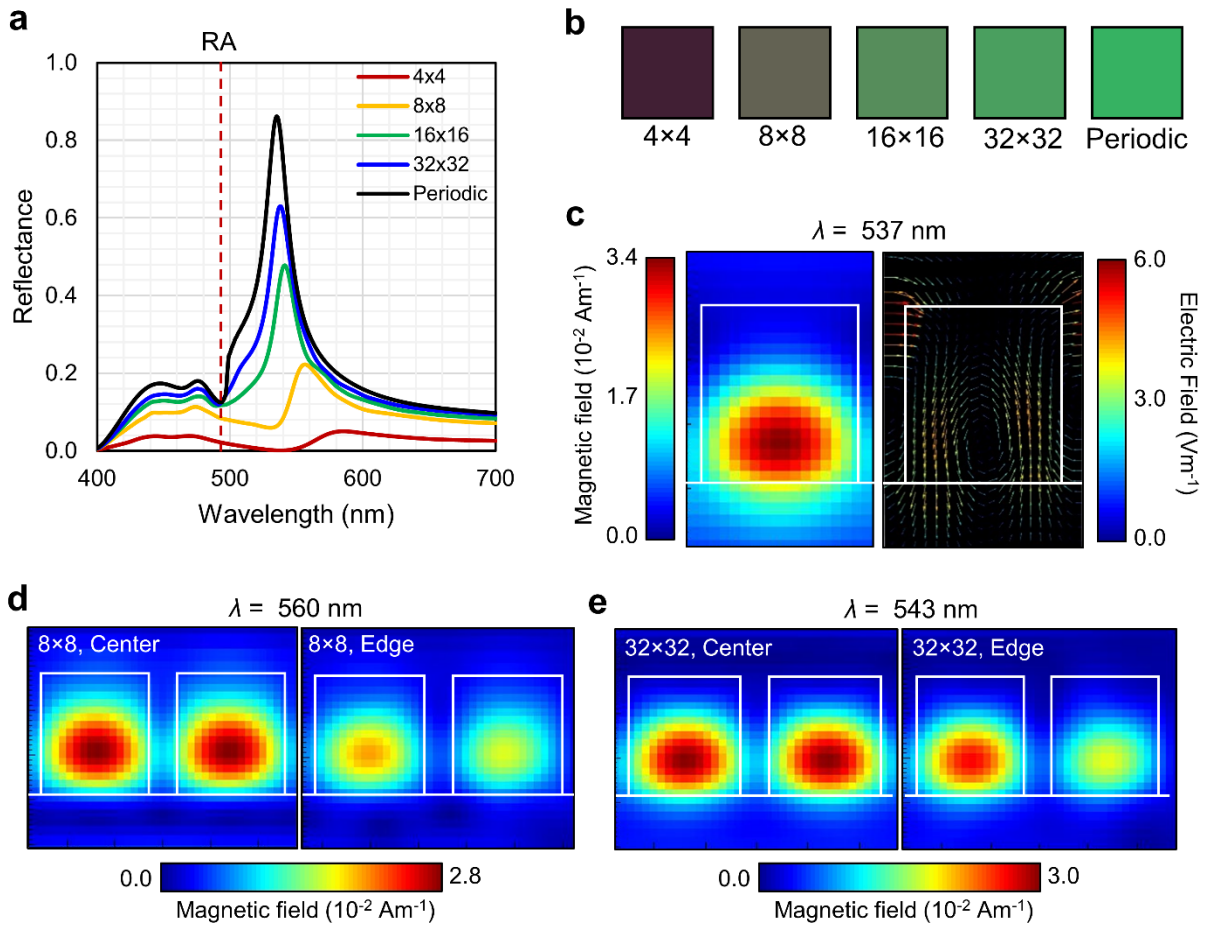


Figure S7. Optical response from different number of structures in arrays. (a) Simulated reflectance of 4x4, 8x8, 16x16, 32x32, and infinite periodic arrays of GaN nanorods with $P = 280 \text{ nm}$, $f = 0.4$, and $h = 250 \text{ nm}$ on an Al_2O_3 substrate. (b) Colour palettes of the 4x4, 8x8, 16x16, 32x32, and infinite periodic GaN nanorod arrays. Field distributions of the (c) infinite periodic array at $\lambda = 537 \text{ nm}$, (d) 8x8 array at $\lambda = 560 \text{ nm}$, and (e) 32x32 array at $\lambda = 543 \text{ nm}$.

Supplementary Note 8 – GaN nanorods with a capping layer

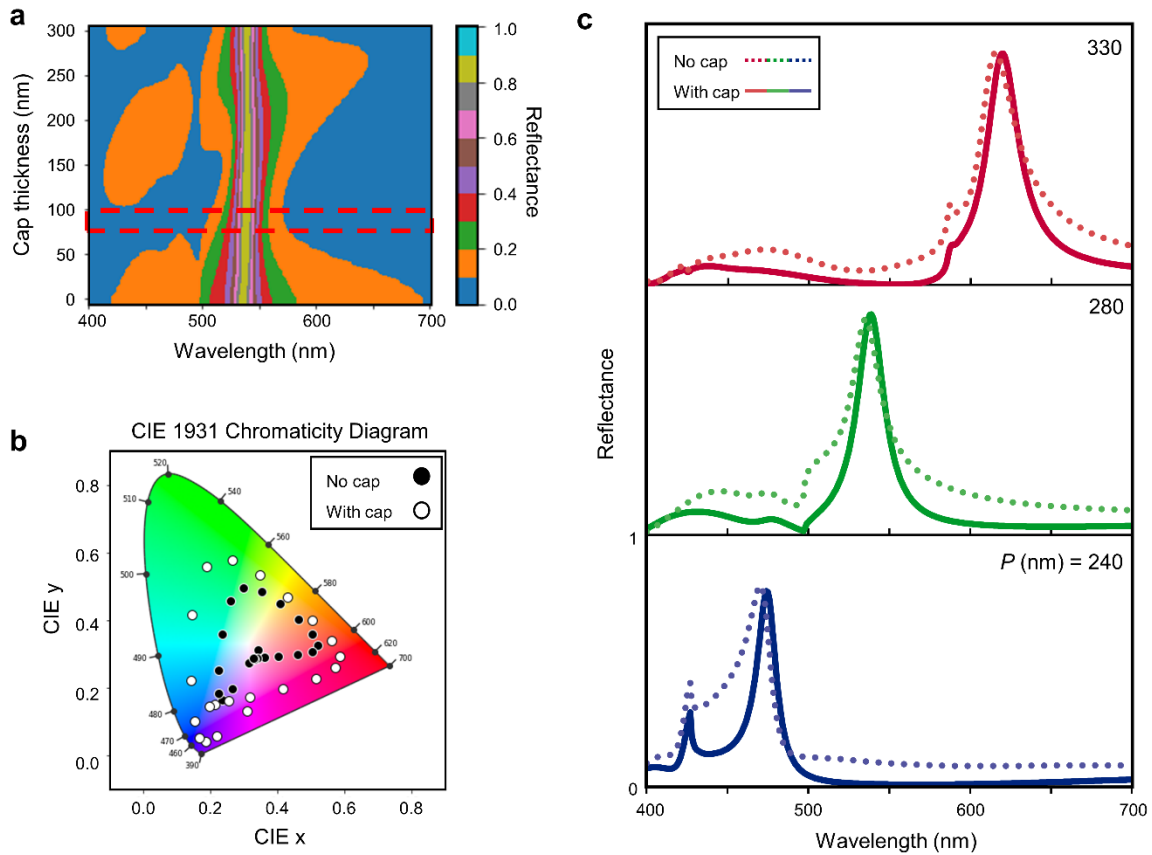


Figure S8. Effect of a capping layer. (a) Simulated reflectance heat map for GaN nanorods with $P = 280$ nm, $f = 0.4$, and $h = 250$ nm on an Al_2O_3 substrate, with an SiO_2 capping layer with varying thickness. The red box indicates where the background is the lowest over all wavelengths, thereby producing the purest colour. (b) Comparison of colour gamut shown on the CIE 1931 Chromaticity Diagram for bare GaN nanorods (black dots) and GaN nanorods with a 100 nm thick SiO_2 capping layer for $P = 200 - 400$ nm. (c) Calculated spectra for GaN nanorods for red, green, and blue colours, with (solid line) and without (dotted line) a 100 nm thick SiO_2 capping layer. The background is suppressed significantly leading to a greatly enhanced purer colour.

To investigate the effect of a capping layer on top of the GaN nanorods, a cap made up of SiO_2 was chosen due to its availability in the two-step fabrication process. Using a GaN nanorod with $P = 280$, $f = 0.40$, and $h = 250$, the effect of a capping layer with thickness from 0 – 300 nm was calculated (Fig. S8a). It can be seen that for a cap of height ~ 100 nm the off-resonance background reflection is suppressed, this leads to an increase in the purity of the produced colour. This is true over for all nanorods with $P = 200 - 400$ nm (Fig. S8b), producing an extended gamut that by far extends the range of achievable colour. The calculated reflection spectra (Fig. S8c) for red, green, and blue show that the resonance peak

is maintained while the off-resonance background is suppressed. This is of great benefit for structural colour.

To understand the mechanism behind this more deeply, multipole scattering modes (up to quadrupole) were calculated (Fig. S9). The dimensions of the GaN nanorod were kept the same as previously, with a 100 nm thick capping layer of varying refractive index from 1.1 to 2.1. As the refractive index of the capping layer increases, the peak in reflection becomes sharper and more well defined, particularly at the tails of the peak, while the background is suppressed almost completely on the red wavelength side for $n = 1.7$ and above. As the refractive index of the capping layer increases, the ED and MQ modes barely change, while the MD resonance is enhanced slightly, with a small blue shift. Interestingly, the biggest change in the multipole modes comes from the EQ, which is enhanced almost 4-fold from the bare GaN nanorod to the $n = 2.1$ capping layer.

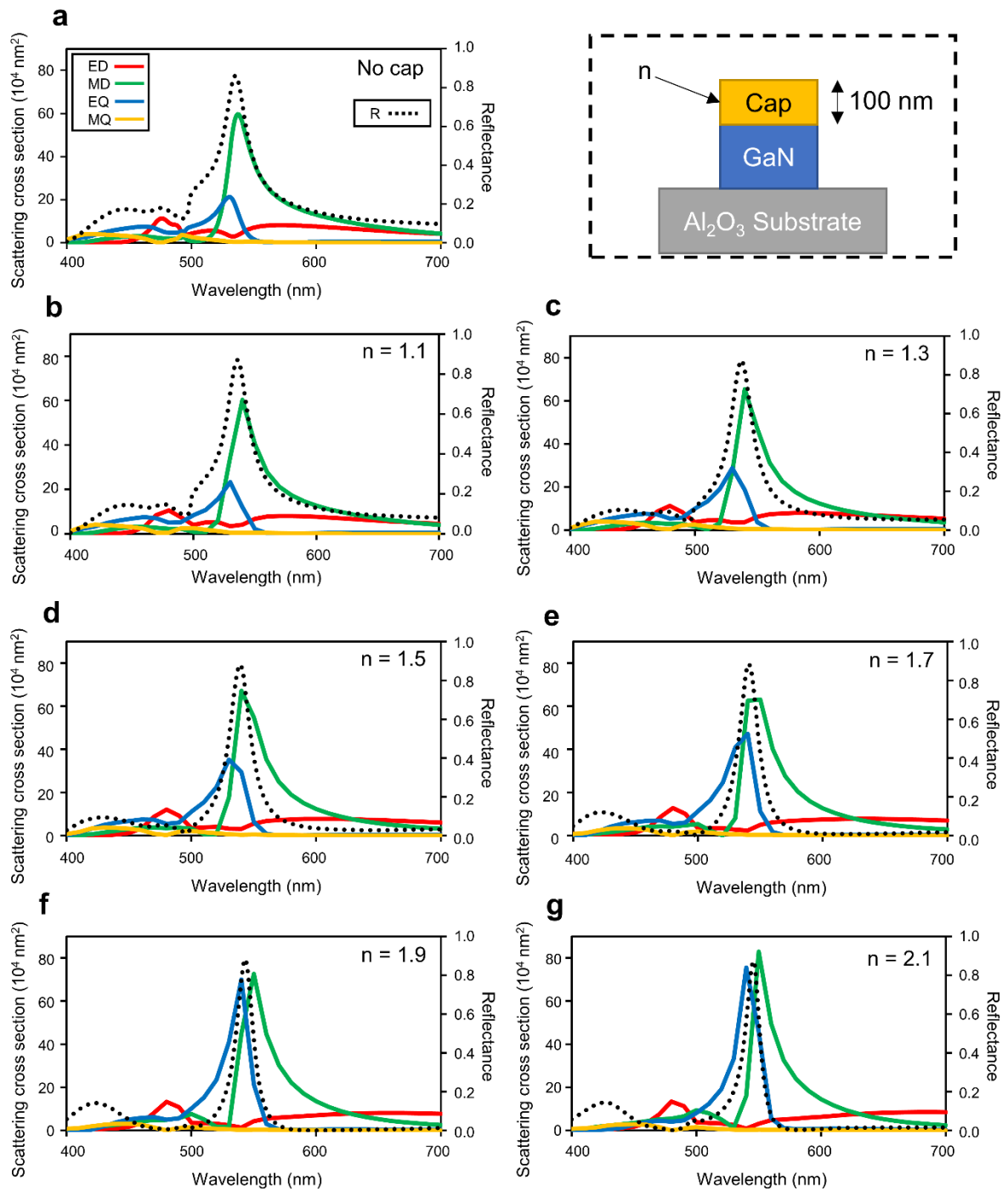


Figure S9. Effect of the refractive index of a capping layer on the reflection and multipole modes. A schematic of the GaN nanorod with a capping layer is depicted in the top right. Calculated reflection, electric and magnetic dipole (ED, MD), and quadrupole (EQ, MQ) modes with (a) no capping layer, and a 100 nm capping layer with refractive index of (b) 1.1, (c) 1.3, (d) 1.5, (e) 1.7, (f) 1.9, and (h) 2.1.

The multipole modes were calculated using the commercially available finite element method (FEM) software COMSOL Multiphysics as

$$\begin{aligned}
D_\alpha^e &= -\frac{1}{i\omega} \int_V d^3\mathbf{r} \left\{ j_0(kr)J_\alpha + \frac{k^2}{2} [3(\mathbf{r} \cdot \mathbf{J})r_\alpha - r^2J_\alpha] \frac{j_2(kr)}{(kr)^2} \right\}, \\
D_\alpha^m &= \frac{3}{2} \int_V d^3\mathbf{r} (\mathbf{r} \times \mathbf{J})_\alpha \frac{j_1(kr)}{kr}, \\
Q_{\alpha\beta}^e &= -\frac{3}{2i\omega} \int_V d^3\mathbf{r} \left\{ \left[r_\alpha J_\beta + r_\beta J_\alpha - \frac{2}{3}(\mathbf{r} \cdot \mathbf{J})\delta_{\alpha\beta} \right] \frac{j_1(kr)}{kr} \right. \\
&\quad \left. + \frac{2k^2}{3} [5(r \cdot \mathbf{J})r_\alpha r_\beta - r^2(r_\alpha J_\beta + r_\beta J_\alpha) - r^2(\mathbf{r} \cdot \mathbf{J})\delta_{\alpha\beta}] \frac{j_3(kr)}{(kr)^3} \right\}, \\
Q_{\alpha\beta}^m &= \frac{5}{2} \int_V d^3\mathbf{r} [r_\alpha(\mathbf{r} \times \mathbf{J})_\beta + r_\beta(\mathbf{r} \times \mathbf{J})_\alpha] \frac{j_2(kr)}{(kr)^2}
\end{aligned}$$

where D_α^e , D_α^m , $Q_{\alpha\beta}^e$, $Q_{\alpha\beta}^m$ are electric dipole, magnetic dipole, electric quadrupole, magnetic quadrupole, respectively, $\alpha, \beta = x, y, z$, $\mathbf{J} = -i\omega(\varepsilon - \varepsilon_h)\mathbf{E}$ is the induced current density, $\varepsilon(\mathbf{x}, \omega)$ and ε_h are the permittivity of the scatterer and the host medium (air), and $j_n(z)$ is the spherical Bessel function. The radiation power is given as $P = \frac{1}{\varepsilon_h^2} \frac{k^4}{12\pi\eta} \sum_\alpha |D_\alpha^e|^2 + \frac{1}{\varepsilon_h^2} \frac{k^6}{12\pi\eta} \sum_{\alpha\beta} |Q_{\alpha\beta}^e|^2 + \eta^2 \frac{k^4}{12\pi\eta} \sum_\alpha |D_\alpha^m|^2 + \eta^2 \frac{k^6}{12\pi\eta} \sum_{\alpha\beta} |Q_{\alpha\beta}^m|^2$, where η is the wave impedance of the host medium. The scattering cross-sections are given as the radiation power divided by the power flux of the incident planewave, $E_0^2/(2\eta)$.